Investigating Tip−Nanoparticle Interactions in Spatially Correlated Total Internal Reflection Plasmon Spectroscopy and Atomic Force Microscopy

Rebecca L. Stiles,[†] Katherine A. Willets,[†,‡] Leif J. Sherry,[§] Jennifer M. Roden, and Richard P. Van Duyne*

Department of Chemistry, Northwestern University, 2145 Sheridan Road, Evanston, Illinois 60208

Received: March 9, 2008; Revised Manuscript Received: May 20, 2008

A new approach for achieving spatially correlated localized surface plasmon resonance (LSPR) spectroscopy and atomic force microscopy (AFM) imaging based on through-the-objective white light total internal reflection (TIR) is described. Using this technique, we successfully demonstrate spatially correlated measurements as well as the effect of tip−nanoparticle interactions including the ability to controllably manipulate nanoparticle position. Significant red shifts are observed in the LSPR spectra of single nanoparticles with successive AFM scans in ambient conditions. Identical experiments performed under water conclusively show that the shifts are caused by the small amount of water that collects between the tip and the sample in ambient AFM.

Introduction

Noble metal nanoparticles have been shown to play an important role in investigations of surface-enhanced spectroscopies,[1–5] chemical and biological sensors,[6–13] and novel plasmonic devices.[14–20] These applications arise from the ability of the nanoparticles to interact with electromagnetic radiation, causing coherent oscillations of the conduction electrons in a phenomenon known as localized surface plasmon resonance (LSPR).[21,22] The spectral properties of these resonances are known to be extremely sensitive to the composition,[23,24] size,[21,25] shape,[21,26–30] external environment,[7,11,21,31–33] and interparticle distances[16,19,31,34–36] of the metallic nanoparticles. While the composition, external environment, and interparticle distances can be readily manipulated, it is much more challenging to reproducibly control the size and shape of individual particles.[29,37,38] Most spectroscopic techniques lead to an ensemble measurement which masks the diversity of the sample in that each nanoparticle in the ensemble has its own unique spectroscopic signature with varying LSPR extinction/scattering maxima, spectral linewidths, and even different responses to changes in local environment,[11,26,27] not to mention the added complexity of plasmon coupling.[19,39] Because of these differences, as well as the inherent difficulty of creating samples of monodisperse nanoparticles, it is necessary to move beyond ensemble measurements toward single particle techniques. Moreover, there is a strong need for techniques that can measure the LSPR spectrum of an individual nanoparticle while simultaneously characterizing its size and shape at the ∼1 nm level.

In this paper, we describe a new approach for achieving spatially correlated LSPR spectroscopy and atomic force microscopy (AFM) imaging based on through-the-objective white light total internal reflection (TIR). Using this technique, we have successfully demonstrated spatially correlated measurements, and, of great importance, the effect of tip-nanoparticle interactions including the ability to controllably manipulate nanoparticle position. As nanoscience turns its focus beyond singular measurements toward developing correlated optical and structural techniques, it is imperative that there is a detailed understanding of how a scanning probe interacts with a nanoparticle surface and possibly alters its optical properties.

Experimental Methods

Chemicals. Hydrogen peroxide (ACS grade), ammonium hydroxide, and sodium citrate from Mallinckrodt Chemicals, silver nitrate (ACS grade) and sodium borohydride (99%) from Sigma Aldrich, sulfuric acid from EMD Chemicals Inc., polystyrene beads from Invitrogen Molecular Probes, and bis(p-sulfonatophenyl) phenylphosphine dihydrate dipotassium from Strem Chemicals Inc. were used as received. Water was purified using a Millipore Milli-Q system (18 MΩ).

Sample Preparation. Glass microscope slides (Fisher Scientific, 12-546) were cleaned with a 3:1 sulfuric acid/hydrogen peroxide solution then base treated with a 5:1:1 water/ammonium hydroxide/hydrogen peroxide solution, resulting in a negatively charged surface, and were then used as substrates for all experiments. Samples patterned with nanosphere lithography (NSL) were prepared by a previously published method[40] involving thermal deposition of silver on top of a mask of polystyrene spheres which are later removed from the surface by sonication in ethanol. For single particle studies, silver nanoprisms were prepared using the method published by Mirkin et al.[29] Briefly, citrate reduced silver seed particles are capped with the stabilizing agent, bis(p-sulfonatophenyl) phenylphosphine dihydrate dipotassium, and then irradiated with a conventional white light source with a 550 nm light bandpass filter (Intor Inc., 550.0-40-75-) for 4−6 h. Over time the solution undergoes color changes that indicate the seed particles are transformed into triangular nanoprisms. The silver nanoprisms, suspended in water, are then dropcast onto the glass substrates and dried in nitrogen.

Instrumental Details. Full instrumental details including an instrument schematic can be found in the Supporting Information, however, a few important details are provided here for the reader. White light from a tungsten-halogen lamp (Ocean

* To whom correspondence should be addressed. Email: vanduyne@chem.northwestern.edu. Tel: (847) 491-3516. Fax: (847) 491-7713.

[†] These two authors contributed equally to this project.

[‡] Current address: Department of Chemistry, The University of Texas at Austin, Austin, TX.

[§] Current address: The CNA Corporation, Alexandria, VA.

10.1021/jp802066b CCC: $40.75
Published on Web 07/12/2008

Optics DH-2000) is directed through a 400 μm diameter core multimode fiber (Ocean Optics) and then quasi-collimated by two lenses at the fiber output. This white light is then directed into the back port of a Nikon TE-2000U inverted microscope where it is reflected off a 50/50 beamsplitter and directed upward through a Nikon 1.45 numerical aperture 60×TIRF oil-immersion objective. An Agilent/Molecular Imaging PicoPlus AFM with a microscope stage adaptor is mounted to the Nikon microscope for AFM imaging. The AFM scanner has a custom-installed IR diode feedback laser, which prevents spectral interference for plasmon measurements. A short-pass filter from Semrock (FF01-750/SP-25) is placed in the path of the scattered light to reject the IR laser while transmitting scattered light from 380 to 720 nm. A prism then directs the scattered light to a PI-Acton Spectra-Pro SP2500i spectrometer which is equipped with a 150 groove/mm grating. The dispersed light is then sent to a PI-Acton liquid nitrogen cooled Spec-10 CCD camera for spectral acquisition.

Results and Discussion

The most widely used method to measure single nanoparticle LSPR spectra is dark field light-scattering microscopy/spectroscopy in which white light is introduced to the sample at a high angle, and the scattered light is collected at a lower angle. There are several experimental configurations for performing dark field measurements with the most common approach using a dark field high numerical aperture condenser in transmission geometry with a low numerical aperture objective to collect the scattered light.[11,27,33,41] A second approach is prism TIR, in which the high angle light is introduced to the sample via a prism mounted at the sample interface; again, an objective is located below the sample to collect the scattered light.[42] In both of these geometries, the excitation and scattered light collection optics block both sides of the sample, and, consequently, it is impossible to perform simultaneous scanning probe structural measurements, such as AFM.[41] A third approach is to use a specially designed dark field scattering microscope objective, serving the dual function of bringing the high angle excitation light to the sample as well as collecting the low angle scattered light, which only needs to contact one side of the sample, leaving the other plane accessible.[43] However when the AFM tip is in contact with the sample, the cantilever on which the tip is mounted and the tip itself scatter the excitation light very strongly, effectively dominating the scattering signal from the sample and preventing real time correlated structural and spectral measurements.

Because of these limitations of sample access and background scattering, most correlated structural and spectral measurements rely upon pattern matching in order to assign a particular structure to a given spectrum.[41,43,44] Even with alignment markers, pattern matching is tedious and does not readily allow for repeated switching between the two measurement schemes making it difficult to interrogate whether the optical signal from a nanoparticle has changed in response to interaction with a scanning probe tip. Presented here is a preliminary analysis of tip−nanoparticle interactions that occur when the tip is rastered across the nanoparticle surface. The results presented demonstrate the importance of being able to analyze the same nanoparticle before and after successive AFM scans, which pattern matching does not allow one to do.

Here we introduce a new approach for collecting spatially correlated optical and structural data on single metallic nanoparticles in parallel and in real-time without the need for pattern matching. This approach is based upon white light through-the-objective total internal reflection,[45] which is analogous to through-the-objective total internal reflection fluorescence (or TIRF) microscopy using laser excitation.[46,47] Figure 1A shows a simple schematic for the experimental setup for white light through-the-objective TIR. White light is introduced through a high numerical aperture microscope objective off-axis, bending the light at sufficiently high angle such that TIR at the air−sample interface is achieved. Excitation of the nanoparticles is accomplished by an evanescent wave generated at this interface, and the low angle scatter can be collected by the same objective. The full instrumental details associated with this setup can be found in the Supporting Information.

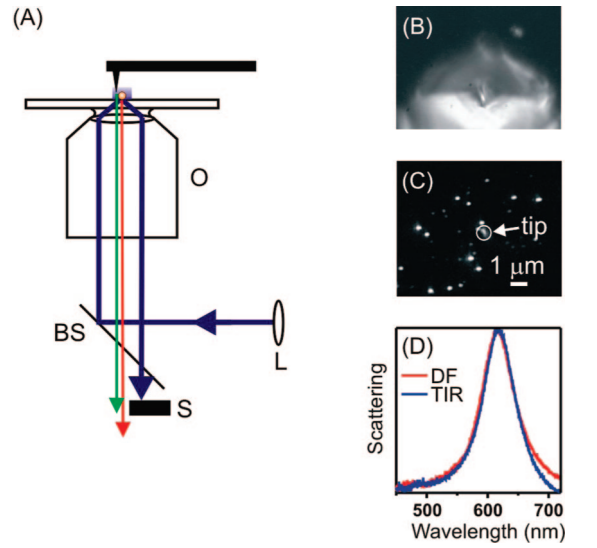

Figure 1. (A) Schematic of the microscope objective/sample/AFM tip interface using white light through-the-objective TIR experiment. Quasi-collimated white light from a tungsten halogen lamp is directed through a 300 mm focal length lens (L) so that it can be bent to an angle greater than the critical angle needed to achieve TIR. The light is then reflected off a 50/50 beamsplitter (BS) and directed upward through a Nikon 1.45 numerical aperture 60× TIRF oil-immersion objective (O). A metal beam stop (S) is placed under the filter turret of the microscope to block the 50% of TIR light that is transmitted through the beamsplitter. In the TIR setup, there is ample room to bring in an AFM tip above the nanoparticle sample which is dropcast on a glass slide. Full instrumental details can be found in the Supporting Information. (B−C) Single nanoparticle scattering image when an AFM tip is in contact with the sample using (B) a dark field scattering objective and (C) the TIR approach. The dark field image (B) is dominated by scattering from the AFM cantilever, while the AFM tip appears only as a diffraction limited spot in the TIR image (C). (D) Comparison of normalized scattering spectra taken using the standard dark field (DF) transmission geometry and the TIR approach.

Panels B and C of Figure 1 compare scattering images of nanoparticles taken using the dark field scattering objective described above and the TIR approach, respectively. In both images, an AFM tip is in contact with the sample. Figure 1B shows clearly that in the dark field geometry the tip scattering completely dominates the image. However, as can be seen in Figure 1C, when the white light through-the-objective TIR approach is used, the tip appears as a diffraction-limited spot alongside the scattering particles. This reduction in the tip scattering is due to the excitation light in the TIR scheme originating from an evanescent wave which exponentially decays in intensity over tens to hundreds of nanometers in the z direction.[46] This exponential decay in the intensity of the excitation field allows the AFM tip to be brought into contact with the sample with no background scattering from the cantilever and significantly reduced background from the tip.

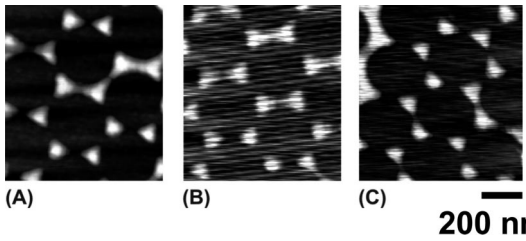

Figure 2. AFM images of a nanosphere lithography fabricated nanoparticle array taken when (A) no microscope objective is in contact with the sample, (B) an oil immersion microscope objective is in contact with the sample, and (C) an oil immersion microscope objective on a vibration isolation mount is in contact with the sample.

With this reduction in background from the AFM cantilever and tip, individual nanoparticles are clearly visible as bright, diffraction-limited spots (Figure 1C).

Using this TIR approach, it can be clearly seen over which particle the AFM tip is scanning over as measurements are taken, thus eliminating the need for any pattern matching. A movie showing a tip scanning over a single nanoparticle sample is included in the Supporting Information. The movie demonstrates how it is possible to know exactly which particle is being probed by the tip at a given moment by synchronizing the acquisition of the optical image with the AFM image. Figure 1D shows that, despite using different microscope configurations, both the dark field scattering and the TIR approach give the same spectroscopic results (with the AFM tip out of contact with the sample). This result is important in that it demonstrates that the white light through-the-objective TIR approach is an equally effective method for illuminating the noble metal nanoparticles to collect spectroscopic information. It should be noted that while the agreement between the two techniques is very good for isotropic nanoparticles, the spectra for anisotropic (multi-peaked) nanoparticles do tend to differ slightly, most likely owing to the differences in the polarization character of the two excitation fields. More discussion on the differences between spectra obtained using dark field scattering and the TIR approach is available in the Supporting Information.

One disadvantage of the TIR approach is that, for TIR to occur, an oil-immersion TIRF objective is required to be in direct contact, through the oil, with the sample substrate so that the numerical aperture of the microscope objective is greater than the refractive index of the sample medium. Unfortunately the sample, being in direct contact with the objective, is thus indirectly in contact with the microscope chassis, the laser table, etc. Currently, the AFM stage is not on a floating table nor is it protected by an acoustic box, and consequently both acoustic and vibrational noise can affect the AFM images obtained. It should be added that modifications can be made to the instrument (e.g., adding an acoustic box) to further minimize the noise, we just have not taken these steps yet.

The effects of noise were tested by using a nanoparticle array constructed using nanosphere lithography (NSL),[40] a technique that allows one to control the thickness and in-plane width of silver nanotriangles through the selection of the nanosphere diameter (D) and the deposited metal thickness (d_m). Figure 2 shows three different AFM images in AC (acoustic)-AFM mode of the NSL patterned surface with $d_m = 20$ nm. Figure 2A is the image taken when no microscope objective is in contact with the sample, and although there is a small amount of noise owing to not floating the table and lack of an acoustic box, the noise is minimal with the nanotriangles clearly observed. However, as can be seen in the AFM image in Figure 2B, when the oil-immersion TIRF objective is brought into contact with the sample, there is a large increase in the observed noise level as much of the vibrational noise is being transferred through the oil. To minimize this problem, the microscope objective was vibrationally isolated from the rest of the optical microscope by elevating the microscope objective on a home-built vibration isolation mount (see Figure 2-S in the Supporting Information). The mount allows the microscope objective to "float" in a cylinder of Buna-N rubber, which damps any mechanical vibrations being transmitted through the microscope. Substantial success in reducing the noise through this method is presented in Figure 2C which shows an AFM image obtained with the TIRF objective in the vibration isolation mount and in contact with the sample.

After optimizing the LSPR and AFM components of the TIR-LSPR-AFM instrument, our focus shifts to utilizing it to simultaneously collect plasmon scattering and structural characterization data from single nanoparticles with an emphasis on studying tip-nanoparticle interactions. Currently there is little data on how the AFM tip interacts with nanoparticles on a surface, and thus, as correlated optical and structural measurements become more popular, there is a great need to understand this interface. To collect this data, we used silver nanoprisms suspended in water, prepared using the method published by Mirkin et al.[29] The particles were dropcast directly on the base treated glass substrates and dried with nitrogen gas. Figure 3A and B shows an AFM image taken in ambient conditions in AC-AFM mode of a single silver nanoprism synthesized using this method. The corresponding LSPR spectra for the nanoprism shown in Figure 3A and B before AFM scans and after consecutive scans of the AFM tip are displayed in Figure 3C. While the initial LSPR spectrum, before any AFM image is obtained, appears to be a normal scattering response of a single nanoparticle, unusual red-shifts in the LSPR spectrum occurred as the AFM tip was rastered over the nanoparticle. While no discernible change in the particle structure appears in the AFM image (Figure 3A and B), there is distinct red-shifting of the LSPR spectra with each consecutive AFM scan. This trend is reproducibly observed in many trials when single nanoparticles are investigated in ambient conditions using TIR-LSPR-AFM.

With no structural change accompanying the LSPR red shifts, the hypothesis developed to explain them originates from dip-pen nanolithography (DPN).[48] Under ambient conditions, a meniscus of water forms spontaneously between the AFM tip and the surface being investigated. This water meniscus is used to deliver molecules of interest to a surface in the DPN technique. It has been shown previously[25] that immersion of a nanoparticle in a higher refractive index solvent (e.g., water in comparison to air) leads to a red shift in its LSPR spectrum. Thus, the hypothesis presented here is that each time the AFM tip rasters across the surface of the nanoparticle, it drags a small quantity of water over the nanoparticle surface. Furthermore, the water layer is likely to increase with each successive AFM scan and thus explains the continuous red shift of the LSPR spectra obtained after subsequent AFM scans.

To test this hypothesis, the same experiment described above was done under water, using a Teflon cell open on both sides that is screwed directly into the sample plate. To ensure the silver nanoprisms would not be displaced from the surface while under water, the hydrolyzed glass substrate was first reacted with 3-aminopropyltrimethoxysilane (3-APTMS) in methanol to silanize the surface. The silver nanoprisms synthesized in the method described above are passivated by the negatively charged bis(*p*-sulfonatophenyl) phenylphosphine (BSPP) sta-

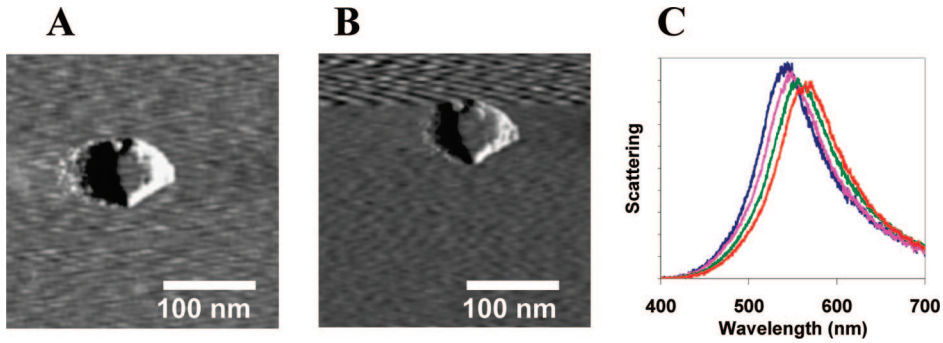

Figure 3. First (A) and seventh scan (B) of an AFM image of a single silver nanoprism. (C) LSPR spectra of the same silver nanoprism before any AFM scans (blue spectrum, furthest blue-shifted) and after three scans of the AFM tip (pink spectrum), five scans (green spectrum), and seven scans (red spectrum, furthest red-shifted).

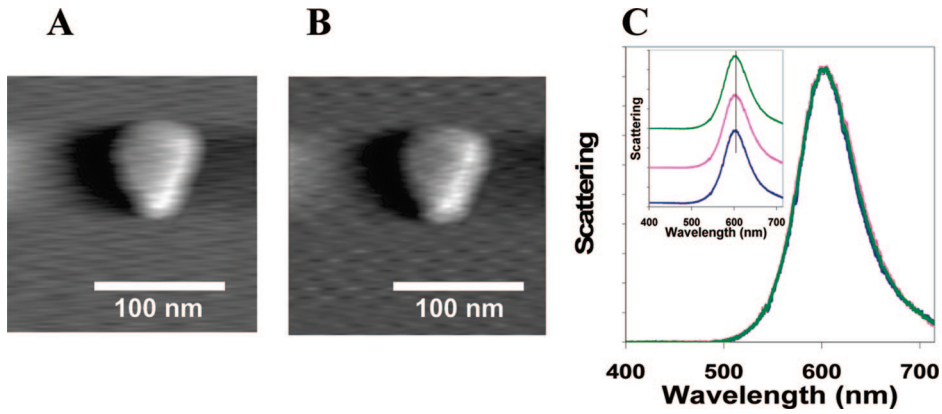

Figure 4. First (A) and eighth scan (B) of an AFM image of a single silver nanoprism under water. (C) LSPR spectra of the same silver nanoprism before any AFM scans (blue spectrum) and after four scans scans of the AFM tip (pink spectrum) and after eight scans (green spectrum). Inset shows the three spectra arbitrarily spaced along the *y* axis with the black line indicating the λ_{max} to show that the spectra are not shifting after AFM scans.

bilizing agent. The negative charges surrounding the nanoparticles cause the particles to electrostatically bind to the partially positively charged silanized glass surface.

Figure 4A and B shows the AFM image of a single nanoprism under water with the AFM in contact mode. Multiple scans of the AFM tip do not cause the particle to move indicating that the electrostatic interaction between the particle and the functionalized surface is sufficiently strong. The LSPR spectra collected before AFM scans and after subsequent scans of the tip over the particle are shown in Figure 4C where it can be clearly seen that no shift in the λ_{max} of the LSPR spectra is observed. This result indicates that when the external dielectric constant is controlled so that it is constant across the surface of the nanoparticle, the AFM tip has no effect on the particle's spectroscopic properties. From these results we can definitively assign the red shifts observed in ambient conditions to the small amount of water that is dragged over the nanoparticle during the AFM scan. This observation also further demonstrates how incredibly sensitive LSPR spectroscopy is to very small changes in the external dielectric constant surrounding the nanoparticle.

While the red-shift of the spectra observed in ambient conditions can now be explained, it is still unknown why the intensity of the LSPR spectra also decreases with subsequent AFM scans in ambient conditions (Figure 3C). Currently there are two hypotheses to explain the intensity decrease; the first is that the very thin water layer that is dragged across the particle by the AFM tip leads to an increase in light scattering in different directions, thus leading to a decrease in collected light, and the second is that the water layer being left behind is nonuniform over the surface of the particle. While extensive modeling has been done regarding the spectroscopic response of a full layer of solvent over a particle,[26,49,50] it has not yet been investigated how the spectra change with nonuniform layers of water over the particle. One can imagine that as the AFM tip, with its water meniscus, rasters over the nanoparticle, it drags the water so that much of it condenses in the last spot of the nanoparticle surface that the tip covers during the scan. Modeling of a nonuniform layer of water on a single nanoparticle is currently underway to better explain the LSPR spectral changes we observe after successive AFM scans.

Finally, we have demonstrated that we can manipulate the position of a single nanoparticle by controllably pushing the particle with the AFM tip. Silver nanoprisms suspended in water were dropcast on hydrolyzed glass and dried with nitrogen gas in the same method described above. The AFM images were taken in ambient conditions with contact mode AFM. The optical feedback of the spatially correlated TIR technique allows us to choose the particle of interest and precisely control its position. Figure 5 shows the diffraction limited spots arising from the scattering of the AFM tip as well as from the particle of interest. With the AFM software, we can controllably position the tip adjacent to the particle of interest (Figure 5A and B), push the particle to the right (Figure 5C), stop the tip and particle on a specified spot (Figure 5D), and finally remove the tip, leaving the particle behind in its new spot (Figure 5E). A full movie of this entire process can be found in the Supporting Information.

While this particle manipulation is still in the early stages of development, one can imagine it becoming an important tool for doing "on-the-fly" lithography in which novel plasmonic

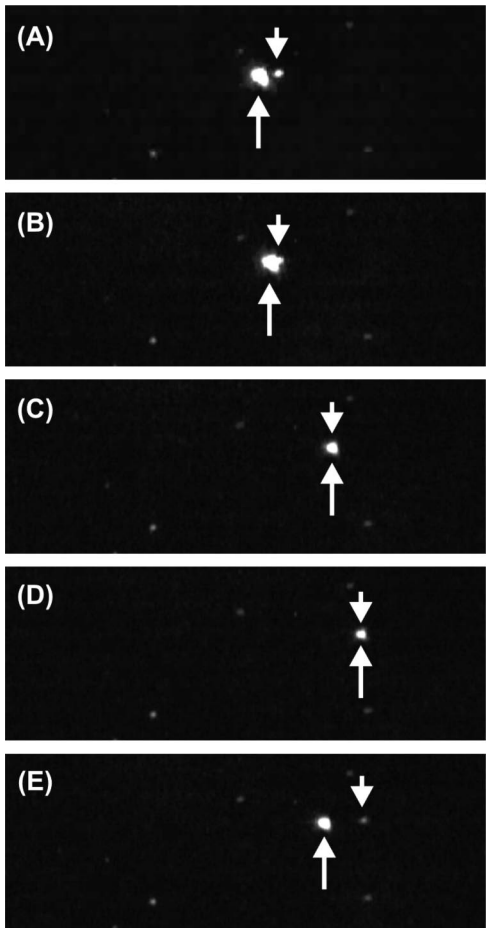

Figure 5. Series of images showing nanoparticle manipulation by an AFM tip. The tip is indicated by an arrow pointing up, while the nanoparticle of interest is indicated by an arrow pointing down. (A) The tip is positioned close to the nanoparticle of interest. (B) The tip is moved adjacent to the nanoparticle in preparation for manipulation. (C) The tip travels across the sample, pushing the nanoparticle with it. (D) The tip is stopped at some final position. (E) The tip is moved away from the nanoparticle, leaving the nanoparticle in its new position. Other nanoparticles in the image have not changed their position and can be used as reference markers to show that only the nanoparticle of interest has been relocated. The intensity of the particle changes due to the nonuniform evanescent field decay length of the excitation light across the field of view.

structures can be developed by combining different types (shape, material, size, etc.) of nanoparticles. Moreover, unlike e-beam lithography, which creates fixed structures, these structures will be dynamic, allowing us to make changes depending on our desired plasmonic properties. To improve this tool, we plan on exploring different surface chemistries as well as particle and tip functionalizations.

Conclusions

In conclusion, we have demonstrated the ability to perform spatially correlated spectral and structural measurements using a through-the-objective white light TIR approach and consequently have been able to investigate tip−nanoparticle interactions in greater detail than previously reported. We are able to measure scattering spectra from single metallic nanoparticles using the evanescent wave from the TIR excitation light, which decays such that we observe no scattering from the AFM cantilever when the AFM tip is in contact with the sample. This approach allows us to not only assign an LSPR spectrum to a particular nanostructure but also to monitor tip-nanoparticle interactions in real time. We have demonstrated that the LSPR of a single nanoparticle is so sensitive to its environmental surroundings that we observe in ambient conditions a continuous red shift in the LSPR spectra with successive scanning of the AFM tip over the nanoparticle. By performing the same experiment under water, we have conclusively shown that the red shift observed in the LSPR spectra after AFM scans is due to the small collection of water between the tip and the surface being dragged over the nanoparticle. This result is important for correlated LSPR and structural measurements as it indicates the significance of keeping the external dielectric constant uniform across the particle's surface. Lastly, we have shown the ability to manipulate the position of a nanoparticle using the AFM tip. Future experiments will focus on understanding the details of the relationships between nanoparticle structures and LSPR spectra, as well as investigating how the AFM tip's dragging of water over a nanoparticle effects its properties. Additionally, "on-the-fly" plasmon lithography will be used to fabricate dynamic plasmonic devices that will allow us to better understand the properties and design rules necessary for creating devices for actual applications.

Acknowledgment. The authors thank Prof. Mark Hersam, Dr. Eddie Foley, and David Andrews for helpful discussions about noise sources in AFM experiments and Prof. George Schatz for helpful discussions regarding LSPR responses of a thin water layer covering the nanoparticle. In addition, we thank David Andrews for assistance with the design of the vibration isolation mount and Dr. Paul Stiles and Jon Dieringer for helpful discussions regarding instrument design. This work was supported by the National Science Foundation (EEC-0647560, CHE-0414554, BES-0507036), the Air Force Office of Scientific Research MURI program (F49620-02-1-0381), DTRA JSTO Program (FA9550-06-1-0558) and the MRSEC program of the National Science Foundation (DMR-0520513) at the Materials Research Center of Northwestern University.

Supporting Information Available: Full instrumental details and movies. This material is available free of charge via the Internet at http://pubs.acs.org.

References and Notes

(1) Haynes, C. L.; Van Duyne, R. P. *J. Phys. Chem. B* **2003**, *107*, 7426–7433.
(2) Kahl, M.; Voges, E.; Kostrewa, S.; Viets, C.; Hill, W. *Sens. Actuator B-Chem.* **1998**, *51*, 285–291.
(3) Campion, A.; Kambhampati, P. *Chem. Soc. Rev.* **1998**, *27*, 241–250.
(4) Freeman, R. G.; Grabar, K. C.; Allison, K. J.; Bright, R. M.; Davis, J. A.; Guthrie, A. P.; Hommer, M. B.; Jackson, M. A.; Smith, P. C.; Walter, D. G.; Natan, M. J. *Science* **1995**, *267*, 1629–1632.
(5) Schatz, G. C.; Van Duyne, R. P. Handbook of Vibrational Spectroscopy; Wiley: New York, 2002; Vol. 1.
(6) Nam, J. M.; Thaxton, C. S.; Mirkin, C. A. *Science* **2003**, *301*, 1884–1886.
(7) Mock, J. J.; Smith, D. R.; Schultz, S. *Nano Lett.* **2003**, *3*, 485–491.
(8) Englebienne, P. *Analyst* **1998**, *123*, 1599–1603.
(9) Haes, A. J.; Chang, L.; Klein, W. L.; Van Duyne, R. P. *J. Am. Chem. Soc.* **2005**, *127*, 2264–2271.
(10) Haes, A. J.; Van Duyne, R. P. *J. Am. Chem. Soc.* **2002**, *124*, 10596–10604.
(11) McFarland, A. D.; Van Duyne, R. P. *Nano Lett.* **2003**, *3*, 1057–1062.
(12) Raschke, G.; Kowarik, S.; Franzl, T.; Sonnichsen, C.; Klar, T. A.; Feldmann, J.; Nichtl, A.; Kurzinger, K. *Nano Lett.* **2003**, *3*, 935–938.
(13) Yonzon, C. R.; Jeoung, E.; Zou, S. L.; Schatz, G. C.; Mrksich, M.; Van Duyne, R. P. *J. Am. Chem. Soc.* **2004**, *126*, 12669–12676.

(14) Andrew, P.; Barnes, W. L. *Science* **2004**, *306*, 1002–1005.
(15) Chapman, R.; Mulvaney, P. *Chem. Phys. Lett.* **2001**, *349*, 358–362.
(16) Haynes, C. L.; McFarland, A. D.; Zhao, L. L.; Van Duyne, R. P.; Schatz, G. C.; Gunnarsson, L.; Prikulis, J.; Kasemo, B.; Kall, M. *J. Phys. Chem. B* **2003**, *107*, 7337–7342.
(17) Leroux, Y. R.; Lacroix, J. C.; Chane-Ching, K. I.; Fave, C.; Felidj, N.; Levi, G.; Aubard, J.; Krenn, J. R.; Hohenau, A. *J. Am. Chem. Soc.* **2005**, *127*, 16022–16023.
(18) Lezec, H. J.; Degiron, A.; Devaux, E.; Linke, R. A.; Martin-Moreno, L.; Garcia-Vidal, F. J.; Ebbesen, T. W. *Science* **2002**, *297*, 820–822.
(19) Maier, S. A.; Kik, P. G.; Atwater, H. A. *Appl. Phys. Lett.* **2002**, *81*, 1714–1716.
(20) Maier, S. A.; Brongersma, M. L.; Kik, P. G.; Meltzer, S.; Requicha, A. A. G.; Atwater, H. A. *Adv. Mater.* **2001**, *13*, 1501+.
(21) Kelly, K. L.; Coronado, E.; Zhao, L. L.; Schatz, G. C. *J. Phys. Chem. B* **2003**, *107*, 668–677.
(22) Willets, K. A.; Van Duyne, R. P. *Annu. Rev. Phys. Chem.* **2007**, *58*, 267–297.
(23) Chan, G. H.; Zhao, J.; Hicks, E. M.; Schatz, G. C.; Van Duyne, R. P. *Nano Lett.* **2007**, *7*, 1947–1952.
(24) Link, S.; Wang, Z. L.; El-Sayed, M. A. *J. Phys. Chem. B* **1999**, *103*, 3529–3533.
(25) Haynes, C. L.; Van Duyne, R. P. *J. Phys. Chem. B* **2001**, *105*, 5599–5611.
(26) Sherry, L. J.; Jin, R. C.; Mirkin, C. A.; Schatz, G. C.; Van Duyne, R. P. *Nano Lett.* **2006**, *6*, 2060–2065.
(27) Sherry, L. J.; Chang, S. H.; Schatz, G. C.; Van Duyne, R. P.; Wiley, B. J.; Xia, Y. N. *Nano Lett.* **2005**, *5*, 2034–2038.
(28) Jin, R. C.; Cao, Y. C.; Hao, E. C.; Metraux, G. S.; Schatz, G. C.; Mirkin, C. A. *Nature* **2003**, *425*, 487–490.
(29) Jin, R. C.; Cao, Y. W.; Mirkin, C. A.; Kelly, K. L.; Schatz, G. C.; Zheng, J. G. *Science* **2001**, *294*, 1901–1903.
(30) Nehl, C. L.; Liao, H. W.; Hafner, J. H. *Nano Lett.* **2006**, *6*, 683–688.
(31) Xu, G.; Chen, Y.; Tazawa, M.; Jin, P. *J. Phys. Chem. B* **2006**, *110*, 2051–2056.
(32) Malinsky, M. D.; Kelly, K. L.; Schatz, G. C.; Van Duyne, R. P. *J. Am. Chem. Soc.* **2001**, *123*, 1471–1482.
(33) Hu, M.; Chen, J.; Marquez, M.; Xia, Y.; Hartland, G. *J. Phys. Chem. C* **2007**, *111*, 12558–12565.
(34) Huang, W. Y.; Qian, W.; El-Sayed, M. A. *J. Phys. Chem. B* **2005**, *109*, 18881–18888.
(35) Gunnarsson, L.; Rindzevicius, T.; Prikulis, J.; Kasemo, B.; Käll, M.; Zou, S. L.; Schatz, G. C. *J. Phys. Chem. B* **2005**, *109*, 1079–1087.
(36) Zhao, L. L.; Kelly, K. L.; Schatz, G. C. *J. Phys. Chem. B* **2003**, *107*, 7343–7350.
(37) Wiley, B.; Sun, Y. G.; Mayers, B.; Xia, Y. N. *Chem.-Eur. J.* **2005**, *11*, 454–463.
(38) Xia, Y. N.; Halas, N. J. *MRS Bull.* **2005**, *30*, 338–344.
(39) Maier, S. A.; Brongersma, M. L.; Kik, P. G.; Atwater, H. A. *Phys. Rev. B* **2002**, *65*.
(40) Jensen, T. R.; Malinsky, M. D.; Haynes, C. L.; Van Duyne, R. P. *J. Phys. Chem. B* **2000**, *104*, 10549–10556.
(41) Michaels, A. M.; Jiang, J.; Brus, L. *J. Phys. Chem. B* **2000**, *104*, 11965–11971.
(42) Fromm, D. P.; Sundaramurthy, A.; Schuck, P. J.; Kino, G.; Moerner, W. E. *Nano Lett.* **2004**, *4*, 957–961.
(43) Mock, J. J.; Barbic, M.; Smith, D. R.; Schultz, D. A.; Schultz, S. *J. Chem. Phys.* **2002**, *116*, 6755–6759.
(44) Jin, R. C.; Jureller, J. E.; Scherer, N. F. *Appl. Phys. Lett.* **2006**, *88*.
(45) Kalkbrenner, T.; Hakanson, U.; Sandoghdar, V. *Nano Lett.* **2004**, *4*, 2309–2314.
(46) Axelrod, D.; Hellen, E. H.; Fulbright, R. M. *Topics Fluoresc. Spectrosc.* **1992**, *3*, 289–343.
(47) Sarkar, A.; Robertson, R. B.; Fernandez, J. M *Proc. Natl. Acad. Sci. U.S.A.* **2004**, *101*, 12882–12886.
(48) Piner, R. D.; Zhu, J.; Xu, F.; Hong, S. H.; Mirkin, C. A. *Science* **1999**, *283*, 661–663.
(49) Whitney, A. V.; Elam, J. W.; Zou, S.; Zinovev, A. V.; Stair, P. C.; Schatz, G. C.; Van Duyne, R. P. *J. Phys. Chem. B* **2005**, *109*, 20522–20528.
(50) Jensen, T. R.; Duval, M. L.; Kelly, K. L.; Lazarides, A. A.; Schatz, G. C.; Van Duyne, R. P. *J. Phys. Chem. B* **1999**, *103*, 9846–9853.

JP802066B